Polymer 51 (2010) 222–231

Contents lists available at ScienceDirect

Polymer

journal homepage: www.elsevier.com/locate/polymer

Deformation behavior of banded spherulite during drawing investigated by simultaneous microbeam SAXS–WAXS and POM measurement

Yoshinobu Nozue [a,*], Yuya Shinohara [b], Yasuo Ogawa [b], Tadashi Takamizawa [b], Takashi Sakurai [a], Tatsuya Kasahara [c], Noboru Yamaguchi [a], Naoto Yagi [d], Yoshiyuki Amemiya [b]

[a] Sumitomo Chemical Co., Ltd., Petrochemicals Research Laboratory, 2-1 Kitasode, Sodegaura City, Chiba 299-0295, Japan
[b] Department of Advanced Materials Science, Graduate School of Frontier Sciences, The University of Tokyo, 5-1-5 Kashiwanoha, Kashiwa, Chiba 277-8561, Japan
[c] Rabigh Refining & Petrochemical Co., Product Development Center, Rabigh 21911, Kingdom of Saudi Arabia
[d] Japan Synchrotron Radiation Research Institute, Mikazuki, Hyogo, Japan

ARTICLE INFO

Article history:
Received 14 July 2009
Received in revised form
10 October 2009
Accepted 13 November 2009
Available online 18 November 2009

Keywords:
Microbeam
SAXS
WAXS spherulite deformation

ABSTRACT

The local deformation behavior inside a poly(ϵ caprolacton) (PCL)/polyvinylbutyral (PVB) banded spherulite during drawing was observed by in-situ microbeam small-angle X-ray scattering (SAXS) – wide-angle X-ray scattering (WAXS) – polarized optical microscopy (POM) simultaneous measurements. From experimental results, we found that the local deformation of a PCL/PVB banded spherulite can be divided into four stages. In stage I, disordering of the crystalline structure occurs. In stage II, the disordering of the crystalline structure ceases and disordering of the stacking and coarse slippage of the lamellae occur. In stage III, after the breakdown of the twisted lamella structure, the reconstruction of a long period structure occurs. In stage IV, further lamella slippage occurs. Our results show no evidence of fine slippage at a local region during the drastic decrease in the long period. This strongly indicates that the melting and recrystallization mechanism occurs during the lamella reconstruction of PCL/PVB.

1. Introduction

A full understanding of the deformation behavior of crystalline polymers is one of the most important issues in the field of polymer processing because it is directly related to the understanding of the mechanical strength of polymeric materials. In a static field, semicrystalline polymers generally form hierarchical structures such as lamella stacking structures, fibril structures (in the form of a lamella bundle) and spherulites. Upon drawing, stacked lamellae are highly fragmented and the *c*-axis is oriented in the drawing direction. Recently, based on the measurement of mechanical properties and wide-angle X-ray scattering, Strobl and co-workers proposed sequential four-step deformation mechanism [1]: (1) the onset of isolated slip process, (2) a collective activity of slip, (3) the beginning of crystalline fragmentation, and (4) chain disentanglement resulting in a finite truly irreversible deformation. Surprisingly, it has been reported that critical strains between these steps are almost universal irrespective of polymer structures [2]. However, in spite of many studies on crystalline polymer deformation by various experimental techniques [3–24], a detailed deformation mechanism about the long period reconstruction process during drawing, is still an area of controversy. Corneliussen and Peterlin found that the long period of drawn polyethylene depends not on the initial long period but on the drawing temperature, and they proposed a melting and recrystallization mechanism [3]. Regarding the detailed process of the melting and recrystallization mechanism, Peterlin further proposed a 'micronecking' process in which the folded lamella blocks are partially unfolded before the formation of microfibrils [4]. The results of transmitted electron microscopy (TEM) [6] and neutron scattering [7,9] have supported the melting and recrystallization mechanism for the long period reconstruction. On the other hand, structures with fine slippage and coarse slippage exist in the deformed crystalline polymer under shear, which can be clearly distinguished with two-dimensional small-angle X-ray scattering (SAXS) pattern (see Fig. 1) [25]. In SAXS measurements during deformation, fine- and coarse-slipped structures have often been reported [11–13,23]. Through detailed X-ray pole figure and morphology observations, some researchers have suggested another long period reconstruction mechanism based on the fine slippage: the deformed lamellae, the chain of which undergoes fine slippage, are pinched off, and then fragmentized lamellae are recovered to become non slipped lamellae [12]. While the mechanism of long period reconstruction which occurs during the fragmentation process of lamellae is still

* Corresponding author.
E-mail address: nozue@sc.sumitomo-chem.co.jp (Y. Nozue).

0032-3861/$ – see front matter © 2009 Elsevier Ltd. All rights reserved.
doi:10.1016/j.polymer.2009.11.031

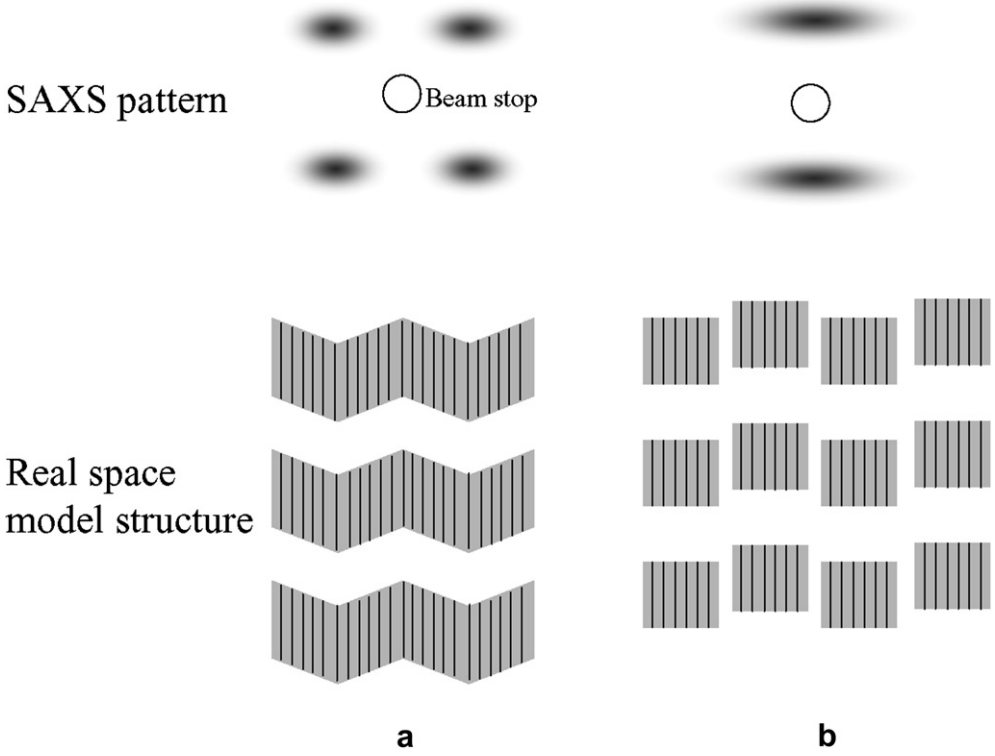

Fig. 1. Illustration of lamellae after fine slippage (a) and coarse slippage (b) and their corresponding SAXS patterns.

debated, it has been recognized that the deformation manner is dependent on various factors such as the drawing temperature and molecular structure of polymers.

There exist various inner structures such as a cross-hatch structure in isotactic PP (iPP) [26] and a twisting lamella structure in many crystalline polymer systems [27–29]. It is interesting to understand the influence of these structures on the deformation manner. We have recently investigated detailed deformation behavior of iPP spherulite with microbeam small- and wide-angle X-ray scattering (SAXS–WAXS) [30]. Microbeam SAXS–WAXS provides the information about wide-scale hierarchical structure at a local region and its spatial distribution with high statistical accuracy, which are hard to obtain with conventional X-ray scattering that provides only averaged structural information. Thus, it is a unique and powerful tool to investigate local structure information in a spherulite and is applied to various materials such as polymeric fibers [31–33], spherulites [34–36], and composites [37]. Deformation mechanism of an isotropically grown structure such as a spherulite is intrinsically inhomogeneous in space [38] and the local deformation behavior should be investigated. By using in-situ microbeam SAXS–WAXS–polarized optical microscopy (POM) measurement during the deformation of an iPP spherulite, we clarified the manner of sequential stress focusing in the cross-hatch structure at a local region of the spherulite [30]. At a local region of an iPP spherulite where the normal of parent lamellae is parallel to the drawing direction, the following sequential deformation process under drawing at 155 °C was found: (1) amorphous part between crystalline lamellae is stretched, (2) crystal packing of parent lamellae is disordered, and (3) the daughter lamellae is reoriented with the fragmentation of the parent and daughter lamellae. During the fragmentation, the long period gradually decreased even though the drawing temperature was about 20 °C higher than isothermal crystallization temperature for the formation of the spherulite. In this experiment, no sign which supports melt and recrystallization mechanism was found.

In the present study, we focus on the deformation behavior of banded spherulite. It is composed of a periodically twisted lamella in the radial direction. The origin of the twisted structure has been widely investigated because of the fundamental interest in the formation of this complex structure [27–29,39–53], and is attributed to the polymer crystal structure such as the asymmetric force on the asymmetric growth front [49,50] and the chiral structure [42,52,53]. It is interesting and important to elucidate how the twisted lamella structure affects the deformation of a spherulite. We apply in-situ microbeam SAXS–WAXS–POM simultaneous measurement to observe the structural changes during drawing in a poly(ϵ caprolacton) (PCL)/polyvinylbutyral (PVB) banded spherulite. PCL/PVB is a characteristic polymer blend; addition of a small amount of PVB to PCL suppresses the nucleation rate of PCL crystal by two orders of magnitude and PCL forms a very large, highly ordered banded spherulite, the band width of which is about 20 μm [29]. Therefore, the PCL/PVB blend is one of the most appropriate model systems for investigating deformation of banded structure in detail by microbeam SAXS–WAXS. By applying microbeam SAXS–WAXS at a local region of a PCL/PVB banded spherulite during drawing, we propose a deformation mechanism of the banded spherulite, which well agrees with four-step deformation mechanism by Strobl and co-workers [1,2].

2. Experimental section

2.1. Materials

PCL and PVB were supplied by Wako Chemicals, Ltd., and were used as received. M_w of PCL was 65,000 and M_w of PVB was 100,000. The PCL/PVB blend sample was prepared by dissolving the desired ratio of PCL to PVB in the common solvent tetrahydrofuran. The PCL/PVB blend ratio used in the experiment was 95/5. The solution sample was cast upon a glass plate at room temperature.

Then, the sample was kept under vacuum at 353 K for 1 day and at 313 K for 1 week.

2.2. Sample preparation for drawing

The solution cast PCL/PVB sample was pressed at 80 °C for 20 min by a compact pressing machine, cooled to 37 °C, and then held for 10–12 h. Although this process was not strictly isothermal crystallization, the induction period of PCL/PVB crystallization at 37 °C was very long (about 5–10 min) and the spherulite hardly grows by the time the temperature of the pressing machine reaches 37 °C (about 10 min). Hence, approximately isothermal crystallization was expected to occur. The thickness of the obtained film was approximately 100 μm and the size of the isothermally crystallized spherulites was 2–3 mm in diameter.

Before the drawing experiment, crystallized film samples were cut into rectangles (10 mm (L) × 2 mm (W) × 0.1 mm (D)) with a notch, and crossed tungsten wires of 20 μm diameter were attached to the sample by applying adhesive tape on the edges of both long sides of the rectangles. The purpose of attaching the crossed wires was to find the position of the X-ray microbeam before the drawing experiment as described later.

2.3. In-situ microbeam SAXS–WAXS–POM simultaneous measurement during drawing

In-situ microbeam SAXS–WAXS–POM experiments were performed at BL40XU, SPring-8 (Hyogo, Japan). The detailed experimental setup is described elsewhere [30]. A quasi-monochromatic X-ray beam ($\Delta E/E \sim 0.02$) from a helical undulator [54] with a wavelength of 0.83 Å was used. A microbeam was obtained by simply inserting a pinhole of 3 μm diameter 15 cm upstream of the sample position. Parasitic scattering was removed by a second pinhole of 50 μm diameter that was inserted immediately before the sample position. The beam size used in this study was about 4 μm × 4 μm in full width at half maximum (FWHM), which was measured by scanning a tantalum knife edge of 100 μm thickness.

The film sample was placed in a temperature-controlled uniaxial drawing machine. The drawing temperature was set at 30 °C in the experiment. The sample was observed under an optical microscope, which was set without obstructing the X-ray path. The position at which the X-ray impinged, the drawing ratio, and the temperature of the sample were controlled from outside the X-ray hutch. SAXS and WAXS images were simultaneously observed using a cooled CCD coupled with an X-ray Image-Intensifier (XRII) [55], and an X-ray flat-panel imager (C9728DK, Hamamatsu Photonics, Ltd., Japan), respectively. The sample-to-detector distances were about 2800 mm and 135 mm for SAXS and WAXS, respectively. The position of the X-ray beam was fixed at an upper region of a spherulite, when the spherulite was stretched in the horizontal direction. The position of the microbeam was determined by using the crossed wires on the sample. When the microbeam passed through the wires, a very strong streak pattern was observed in the SAXS image. By finding the position where the crossed streak pattern was observed, we obtained the rough position of the microbeam. Once this position was identified under a microscope, it was easy to pinpoint the position of the microbeam by irradiating the polymer sample with the X-ray microbeam without using a 1/1000 absorber which was inserted during the measurement, and damaging the sample.

For data acquisition, the following procedure was repeated: (1) a sample was drawn while monitoring the POM image, (2) the drawing was stopped when any change was observed in the spherulite, (3) the sample position was adjusted so that a microbeam hits a fixed position on the spherulite, and (4) SAXS and WAXS images were simultaneously observed. The exposure time was 2 s for both SAXS and WAXS. The SAXS–WAXS measurement was performed within 20 s after stopping the drawing process. The drawing speed was 0.05 mm/s and the initial distance between the chucks was about 6 mm. It should be noted that the drawing speed in the local region of a spherulite was significantly different from the macroscopic drawing speed.

2.4. Analysis of SAXS patterns

Fig. 2(b) shows a raw SAXS pattern of PCL/PVB, where a highly oriented pattern is observed. To analyze the structural deformation of lamellae upon drawing, we extract the sector region of interest from the SAXS pattern, as shown in Fig. 2, and averaged the intensity over the sector. We fitted the obtained one-dimensional scattering profiles with a Gaussian function and then evaluated the long period of the lamellae. The FWHM of the SAXS patterns was calculated from the scattering profiles perpendicular and parallel to the drawing direction. The SAXS peak can be assigned as shown in Fig. 3, which was already reported in our previous scanning microbeam SAXS–WAXS simultaneous measurement [35,36].

2.5. Analysis of WAXS patterns

Fig. 2(c) shows a typical raw WAXS pattern. As shown in this figure, only a partial pattern was obtained, because the detector for WAXS was placed away from the axis of the X-ray beam so as to record both SAXS and WAXS simultaneously. Two reflections, the 110 and 020 reflections, were analyzed to investigate the structural change during drawing. The azimuthal distribution and sector-averaged profiles of each reflection were calculated after

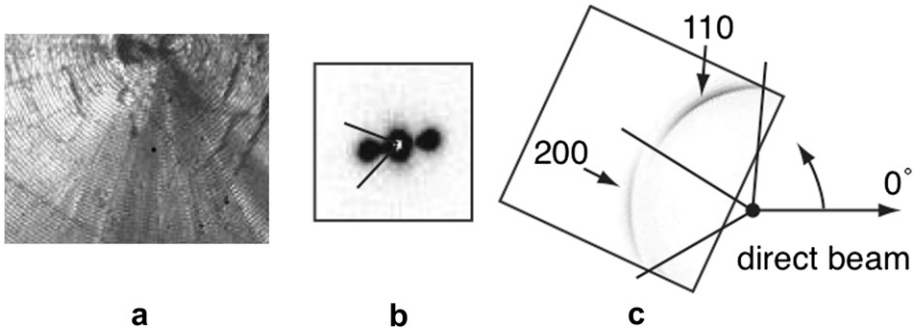

Fig. 2. Typical datasets obtained by POM (a), SAXS (b), and WAXS (c). In the POM image, the position of the microbeam is shown by a dot. The definition of the azimuthal angle is shown in (c).

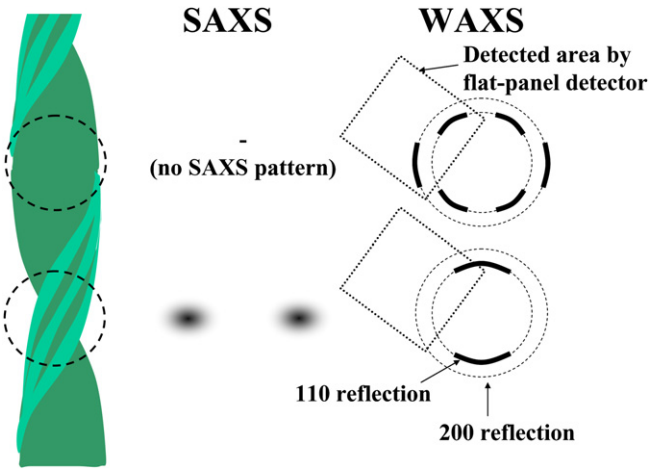

Fig. 3. Illustration of relationship between SAXS, WAXS patterns and twisted structure. This correspondence was reported in our previous publication [35,36].

background subtraction. Each diffraction peak in the sector-averaged profile was fitted with a Gaussian function, and the FWHM of each diffraction peak was obtained. The azimuthal angle was defined as shown in the figure. The WAXS peak can be assigned as shown in Fig. 3, which was already reported in our previous scanning microbeam SAXS–WAXS simultaneous measurement [35,36].

3. Results

3.1. In-situ microbeam SAXS–WAXS–POM measurement during drawing of PCL/PVB

Fig. 4 shows microbeam SAXS–WAXS–POM datasets obtained during the drawing. The black points in the figures indicated the positions of the X-ray microbeam. Before drawing (Fig. 4(a)), anisotropic SAXS and WAXS patterns were clearly observed, indicating that a well-oriented higher-order structure was formed at a very local region of the banded spherulite. The anisotropic SAXS pattern originates from the lamella structure, the plane normal of which is almost perpendicular to the incident X-ray microbeam. In the partial two-dimensional WAXS pattern, one of the four 110 reflections was observed in Fig. 4(a). The 110 reflection arc in Fig. 4(a) mainly originates from the lamella structure, the normal of which is parallel to the incident X-ray microbeam [36].

In Fig. 4, the drastic changes in SAXS and WAXS patterns during drawing are clearly observed. In SAXS, the anisotropic pattern becomes broader and, in particular, the width of the scattering intensity perpendicular to the drawing direction increases during drawing. In the WAXS pattern, the azimuthal position of the 110 reflection, which is initially located at 122°, moved toward 90°, while the 200 reflection correspondingly disappeared during drawing. Through the quantitative analyses of the SAXS and WAXS pattern changes, we found that the deformation process of a PCL/PVB banded spherulite is divided into four stages. Thus, in the following, we show the results of data analyses by relating them to the four stages of deformation.

First, the results of WAXS data analyses are shown. In Fig. 5, the changes in FWHM of the 110 and 200 reflections are shown. From the FWHM of the 110 and 200 diffraction peaks along the radial direction calculated from the sector-averaged WAXS profiles, the order of crystalline structure, which includes the packing order and the crystal size, was evaluated. In stage I, the disordering of crystalline structure was induced by the action of stresses, while no further disordering was observed in stage II. Next, the changes in the azimuthal distribution of 110 and 200 reflections are shown in Fig. 6. It was found that no drastic change occurred in the azimuthal distribution of the 110 reflection until Frame No. 11. At Frame No. 12, which is the boundary between stages II and III, a change in the azimuthal distribution of the 110 reflection clearly occurred, accompanied with the disappearance of the 200 reflection. These results clearly indicate a change in the crystal orientation by the breakdown of the initial twisting structure through the applied stress.

In order to understand the change of the azimuthal distribution of the WAXS pattern during the drawing process, scanning microbeam WAXS was performed. The upper regions of PCL/PVB spherulites before and after drawing were scanned along the radial direction of the spherulite using an X-ray microbeam. In Fig. 7, the change in the azimuthal distribution of the 110 reflection during the scanning of the spherulites is expressed as a contour map. The abscissa is taken as the azimuthal angle and the ordinate as the scanning position. In Fig. 7(a), a contour map obtained from a banded spherulite before drawing is shown, where a periodic change in the azimuthal distribution was clearly observed. It is known that this periodic pattern of the 110 reflection indicates the continuous twisting of the lamella structure [35]. On the other hand, the contour map in Fig. 7(b) shows the azimuthal distribution of the 110 reflection from the spherulite after drawing. The periodic change in the azimuthal distribution is not observed after drawing. The difference between Fig. 7(a) and (b) clearly indicates that the change in the azimuthal distribution of the WAXS pattern in Fig. 6 originates from the breakdown of the periodic twisting structure and the subsequent alignment of the *c*-axis orientation of the crystal along the drawing direction.

Next, the results of SAXS data analyses are shown. The changes in the long period and its FWHM in the SAXS pattern were calculated from sector-averaged one-dimensional profiles (Fig. 8). In stage II, the long period gradually increased, while no clear change in the long period was observed in stage I. In stage III, the long period drastically decreased. This decrease may correspond to the reconstruction of large lamella structure, which will be discussed later. Furthermore, it was also found that the SAXS peak broadened perpendicular to the drawing direction during the drawing (Fig. 4(e)–(g)), and SAXS pattern finally showed the two-bar pattern. Therefore, we analyzed the FWHM of SAXS profiles perpendicular to the drawing direction in each frame (Fig. 9). As shown in the figure, FWHM of the SAXS intensity perpendicular to the drawing direction started to increase in stage II, and this change accelerated in stage III and continued in stage IV. Although the increase in FWHM occurred before the drastic decrease in the long period, the SAXS pattern was not a clear two-bar pattern but was still spotty at stage II though the width gradually broadened. The SAXS pattern indicates that not the fine slippage but the slight coarse slippage of lamellae partially occurs in lamellae, *c*-axis of which are aligned along the drawing direction, before the drastic reconstruction of long period structure (see Fig. 1). For a clearer understanding of stage III, we computed Fourier transforms of the SAXS profiles along the drawing direction in Frame No. 12–14. The enlarged SAXS spots, the one-dimensional SAXS intensity profiles along the radial direction, and the corresponding Fourier transform profiles, i.e., the electron density correlation functions, are shown in Fig. 10. By comparing the Fourier transform profiles, it was found that the electron density correlation between the stacked lamellae in Frame No. 13, which corresponds to the transient state of lamella reconstruction, was weakest among Frame No. 12–14, while the correlation in Frame No. 14, which corresponds to the state after the reconstruction of lamellae, was strongest. This means that the lamella stacking structure after the reconstruction in stage III has a higher electron density correlation

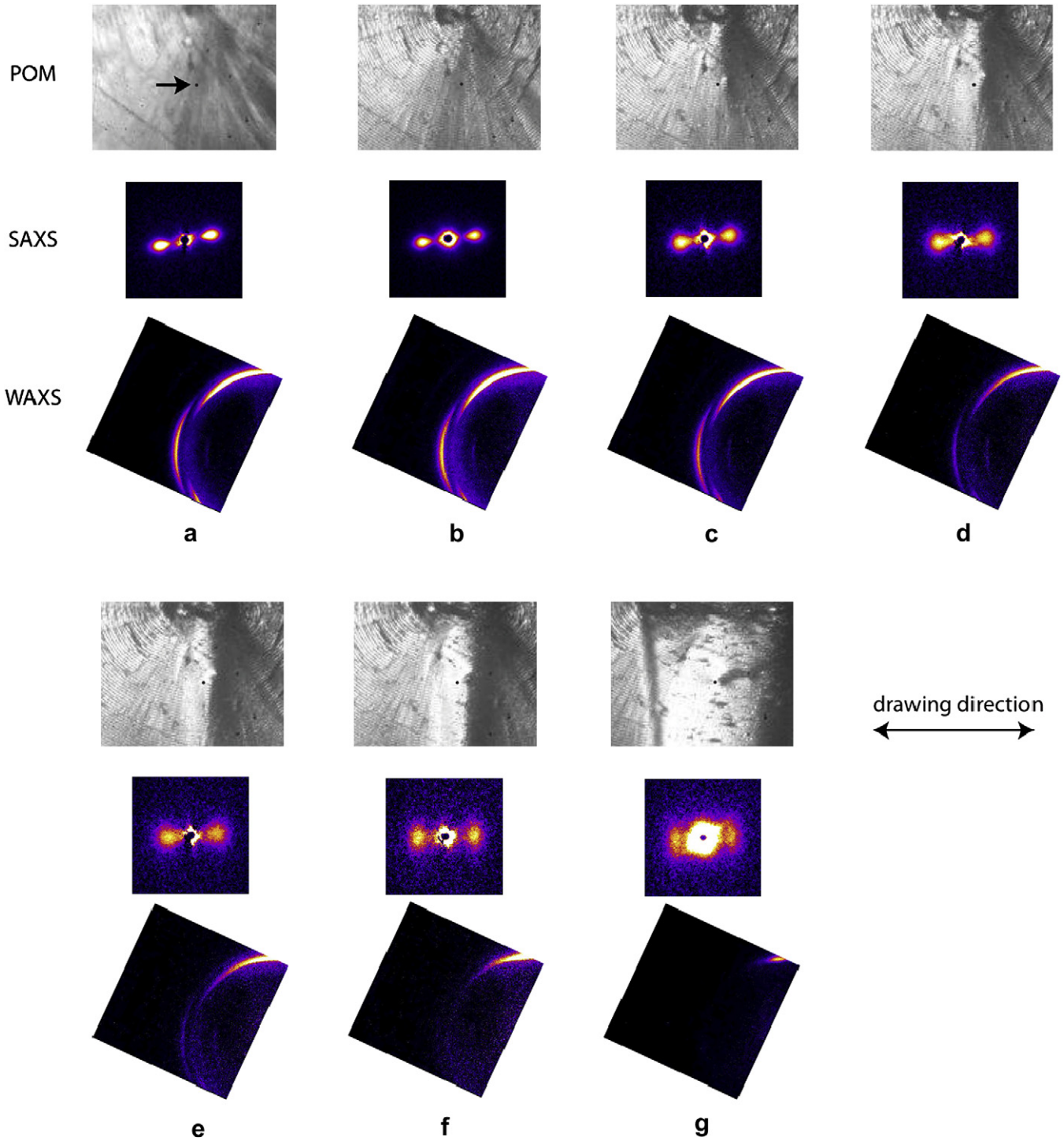

Fig. 4. Representative POM-SAXS-WAXS datasets of PCL/PVB = 95/5 banded spherulite during drawing.

than that before reconstruction. In addition, it should be noted that the correlation function peak in Frame No. 14 is the strongest out of the three frames at its first maximum at 170 Å and second minimum at 220–230 Å. This stronger interference indicates that the uniformity of the long period is higher.

For stage III, it is also interesting to compare the SAXS and WAXS changes. The breakdown of the twisted lamella structure (see the WAXS azimuthal distribution change from Frame No. 11 to Frame No. 12 in Fig. 6) occurred before the drastic decrease in the long period (see the change in the long period from Frame No. 12 to Frame No. 13). This clearly shows that the reconstruction of the long period structure starts after the breakdown of the twisting lamella structure. This seems reasonable because it is difficult to reconstruct the lamella structure without destruction of the twisted lamella structure.

3.2. DSC measurement of PCL/PVB before and after drawing

In the PCL/PVB blend system, a very large spherulite was formed, and the deformed part of the spherulite was easily cut out

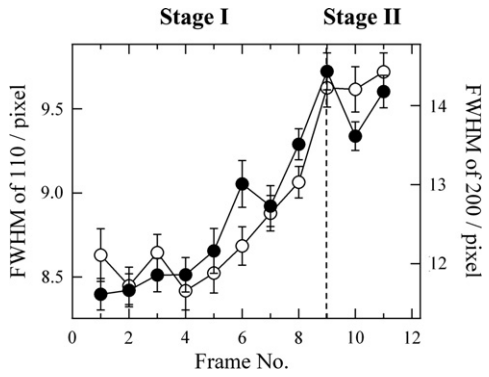

Fig. 5. Changes in FWHM of 110 reflection (open circles) and 200 reflection (closed circles) during drawing.

after drawing. By selecting only the deformed region from a spherulite after drawing for DSC measurement, the thermal property of the reconstructed lamella structure was examined. The melting behavior of PCL/PVB after deformation was compared with that before drawing (isothermally crystallized at 37 °C). Additionally, the melting behavior of the PCL/PVB spherulite crystallized under the isothermal condition at 30 °C, which corresponds to the drawing temperature, was also compared. In Fig. 11, the melting curve of isothermally crystallized PCL/PVB exhibited a single melting peak with a wide distribution of endothermic heat flow. As is well known, a sample isothermally crystallized at a lower temperature has a melting peak at a lower temperature, indicating lower thermal stability due to the formation of thinner lamellae under larger undercooling. Surprisingly, the melting behavior of the drawn PCL/PVB was considerably different from those of the isothermally crystallized samples; the melting peak of the drawn sample was much sharper. Furthermore, the peak melting temperature of the drawn PCL/PVB was lower than that before drawing and was comparable to that of PCL/PVB isothermally crystallized at 30 °C, although the widths of the DSC profiles were significantly different. This strongly indicates that the lamella structure is greatly modified by the drawing procedure, resulting in the reconstruction of lamellae with more uniform and lower thickness. In order to transform lamellae with a wide thickness distribution into those with a narrow thickness distribution, it seems natural to consider the occurrence of melting and recrystallization mechanism [3,4] during drawing. The mechanically melted parts may have a memory of their structure such as their orientation and conformation, and may easily recrystallize from the memorized state like oriented melt at the drawing temperature. In such a case, the melting point of the recrystallized sample should be comparable to that of a sample isothermally crystallized at the drawing temperature. We discuss the deformation mechanism in detail in the final section.

4. Discussion

4.1. PCL/PVB banded spherulite deformation model

On the basis of our experimental results, a structural deformation model during drawing is constructed as shown in Fig. 12. In stage I, disordering of the crystalline structure starts, while no change in the long period and twisting lamella structure occurs. In stage II, the disordering of the crystalline structure ceases, and a gradual increase in the long period starts accompanied with disordering of the stacking (see Fig. 8) and slight coarse slippage (see Fig. 9). At the boundary of stages II and III, the destruction of the twisted lamella structure occurs. In stage III, after the breakdown of the twisted lamella structure, the shortening of the long period structure and further coarse slippage occurs, that is, the reconstruction of the stacked lamella structure starts. During the reconstruction of lamellae in stage III, the thickness distribution of the lamella structure becomes much narrower, which may be caused by the mechanical melting and recrystallization. In stage IV, no clear characteristic was found except for the occurrence of further coarse slippage of the lamellae, and therefore, this stage is omitted in Fig. 12. This four stage model seems to agree with four-step deformation model by Strobl and co-workers [1]. The disordering of crystal packing in stage I will be induced by the isolated chain slippage. The coarse slip of lamellae in stage II will correspond to the collective activity of slippage. The destruction of twisting and drastic change in long period in stage III will correspond to fragmentation process. The further coarse slip in stage IV will be induced by the chain disentanglement.

The sequence of this deformation model seems reasonable. Initially, the stress is focused on disordering of the crystalline structure. After the disordering of the packing, the coarse slippage of lamellae may easily occur. Twisting lamellae, which consists of a disordered structure with coarse slippage, may be then broken down and their *c*-axis may be aligned along the drawing direction.

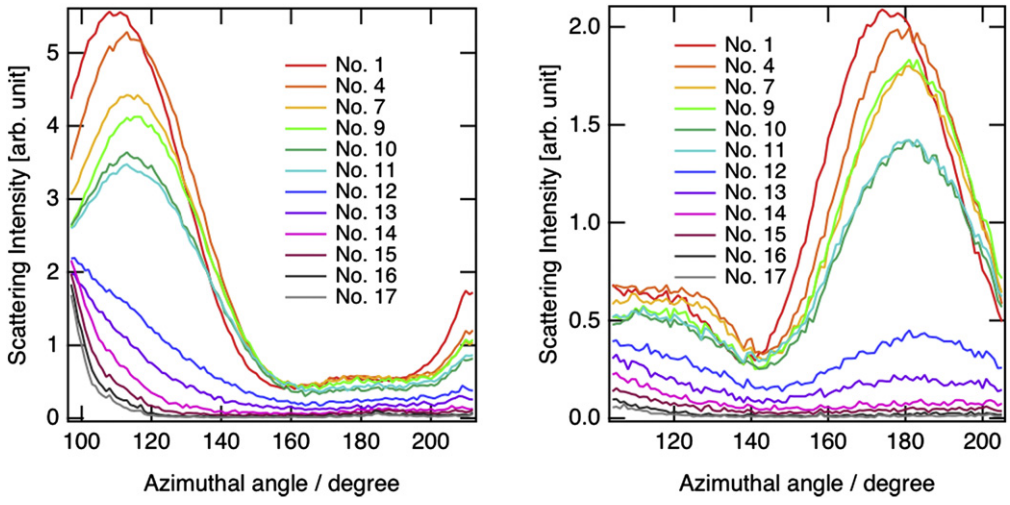

Fig. 6. Intensity map of azimuthal distribution of 110 reflection (left) and 200 reflection (right) during drawing.

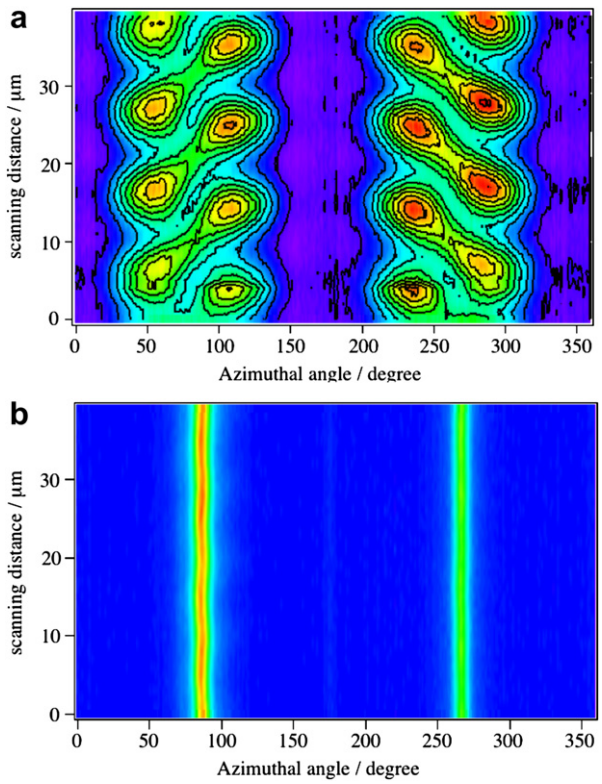

Fig. 7. Intensity map of azimuthal distribution of 110 reflection of PCL crystallized at 37 °C before drawing (a) and after drawing (b).

After the alignment of the *c*-axis of lamellae along the drawing direction, the drastic reconstruction of the lamellae will finally occur. Note that the deformation manner of lamella structures which cannot be detected by microbeam 2D-SAXS and WAXS is still unclear even with our experiment.

4.2. Discussion on melting and recrystallization mechanism

The model of reconstruction of the lamella structure during drawing is still unclear. Peterlin and co-workers suggested a micronecking mechanism involving the melting and recrystallization process of PE, which was based on the results of the melting temperature change during drawing and morphology observation [3,4]. In their experiments, the initial lamella thickness hardly affected the final lamella thickness after drawing, and the final structure was only determined by the drawing temperature. Some authors used small-angle neutron scattering and reported experimental results that supported the melting and recrystallization of PE under some experimental conditions [7,9,10]. On the other hand, from the results of X-ray scattering and morphology observation, other authors suggested a different model for the change in lamella thickness during drawing. They considered the reconstruction of lamella as being due to the fine slippage of lamellae and the recovery from the fragmented slippage state [11–13]. Actually, the lamellae are thinner after fine slippage, and there are several reports in which experimental evidence of fine slippage during the compression of PE sheets is presented [13,14]. In one scenario that rejects the mechanism of melting and recrystallization, the structure is pinched off after the fine slippage, and the fragmented structure with fine slippage is recovered when a strong deformation force is applied [12]. In this scenario, the recovered structure has a different lamella thickness from original lamellae, depending on the angle of tilting and experimental conditions such as the deformation temperature.

We consider that the reason why such a controversy has continued until now is partially due to the limitation of the experimental techniques. Microscopic methods such as TEM cannot easily observe in-situ structural changes in the range of the hierarchical structure, and furthermore, the statistical accuracy is poor. On the other hand, scattering techniques have so far shown only spatially averaged structure information, comprising the superposition of various deformation stages in different regions of spherulites.

The microbeam X-ray scattering technique can overcome such experimental limitations. Actually, in our experiment, we observed the deformation behavior at a very local region with good statistical accuracy. In our results, we did not find any clear evidence for fine slippage at the upper region of the spherulite during a drastic change in the long period. Thus, in the case of lamella reconstruction, where the lamella plane normal is already parallel to the drawing direction, the deformation model based on fine slippage

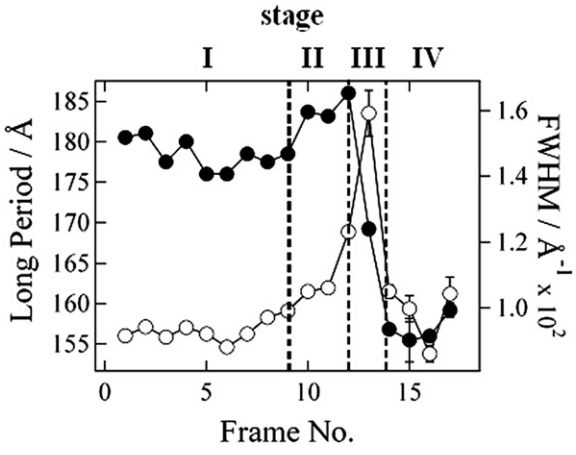

Fig. 8. Change in lamellar long period (closed circles) and FWHM of SAXS intensity profiles along drawing direction (open circles) obtained from the sector-averaged SAXS intensity profiles.

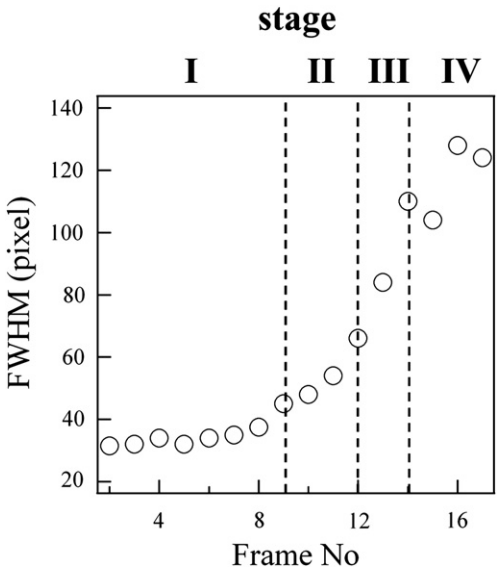

Fig. 9. FWHM of SAXS intensity in the direction perpendicular to the drawing direction during drawing.

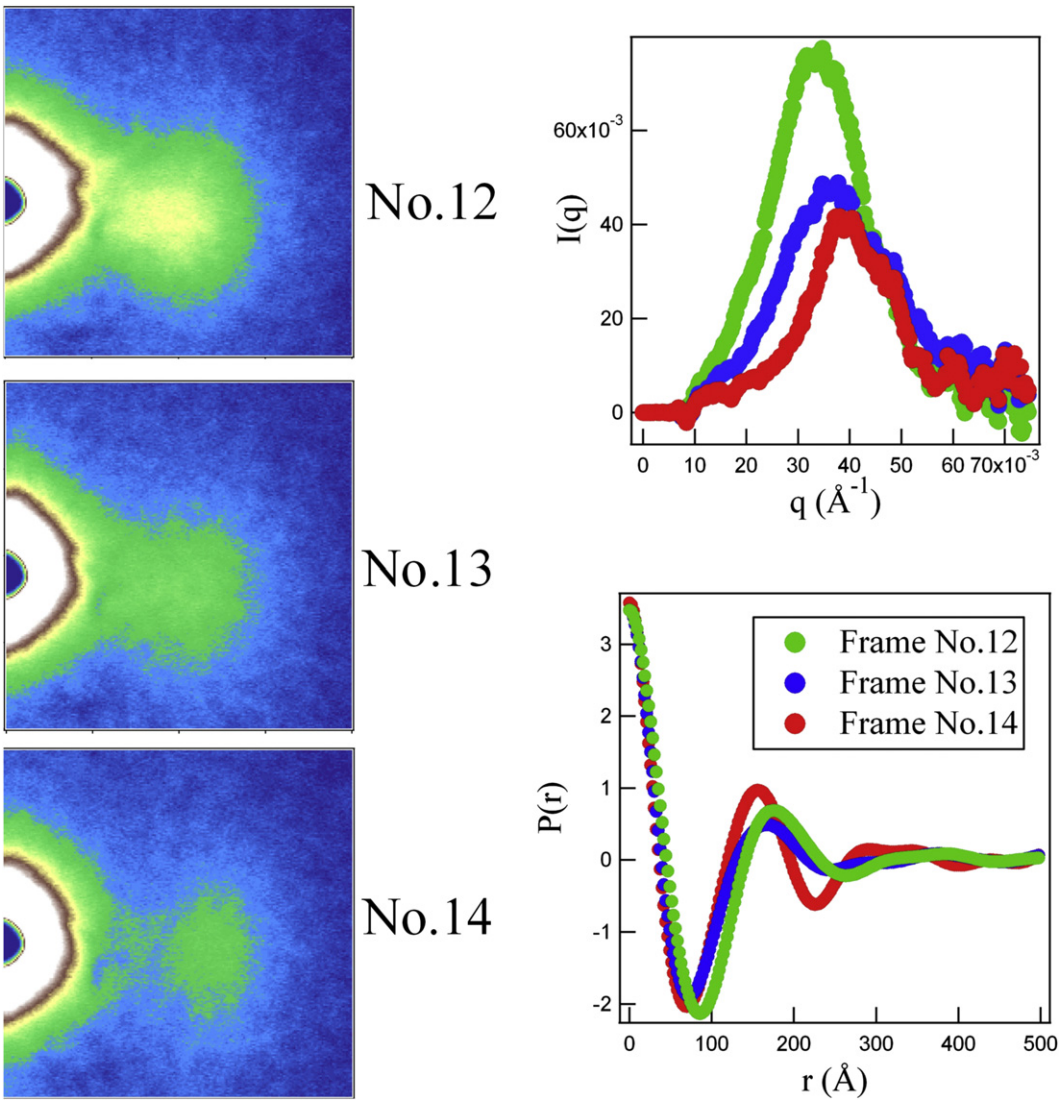

Fig. 10. SAXS pattern change in stage III (left), the extracted one-dimensional profiles (upper right), and Fourier transform of the profiles (lower right).

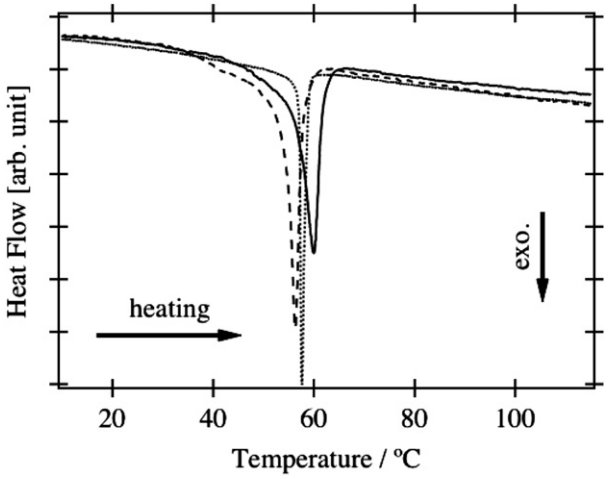

Fig. 11. DSC results for PCL/PVB = 95/5 isothermally crystallized at 37 °C before drawing (solid line), after drawing (dotted line), and PCL/PVB = 95/5 isothermally crystallized at 30 °C (dashed line).

and the recovery process in lamellae is not adequate for explaining the reconstruction of the long period. In this case, drastic coarse slippage accompanied with melting and recrystallization appears to be the only essential process for lamella spacing reconstruction.

By combining our results with previous results, fine slippage is considered as an additional preliminary process in the region where the chain axis of the lamellae is inclined to the drawing direction. In such a region, strong shear stress will be applied to inclined lamellae and the fine slip structure will be formed. When the chain is aligned along the drawing direction via fine slippage, drastic coarse slippage will proceed. Several authors already proposed that double yielding points in stress–strain curve correspond to fine slippage and coarse slippage, respectively [56]. In addition, it should be noted that there is the possibility of fine slippage during the destruction of twisting structure in the lamellae which is not detected by X-ray scattering. In the deformation of a PCL/PVB banded spherulite, the breakdown of twisting at the boundary of stage II and III is also included as a preliminary process, and during the alignment of lamellae, the fine slippage may occur though it cannot be measured with our experimental setup. In the future, the validity of this concept should be examined by further microbeam

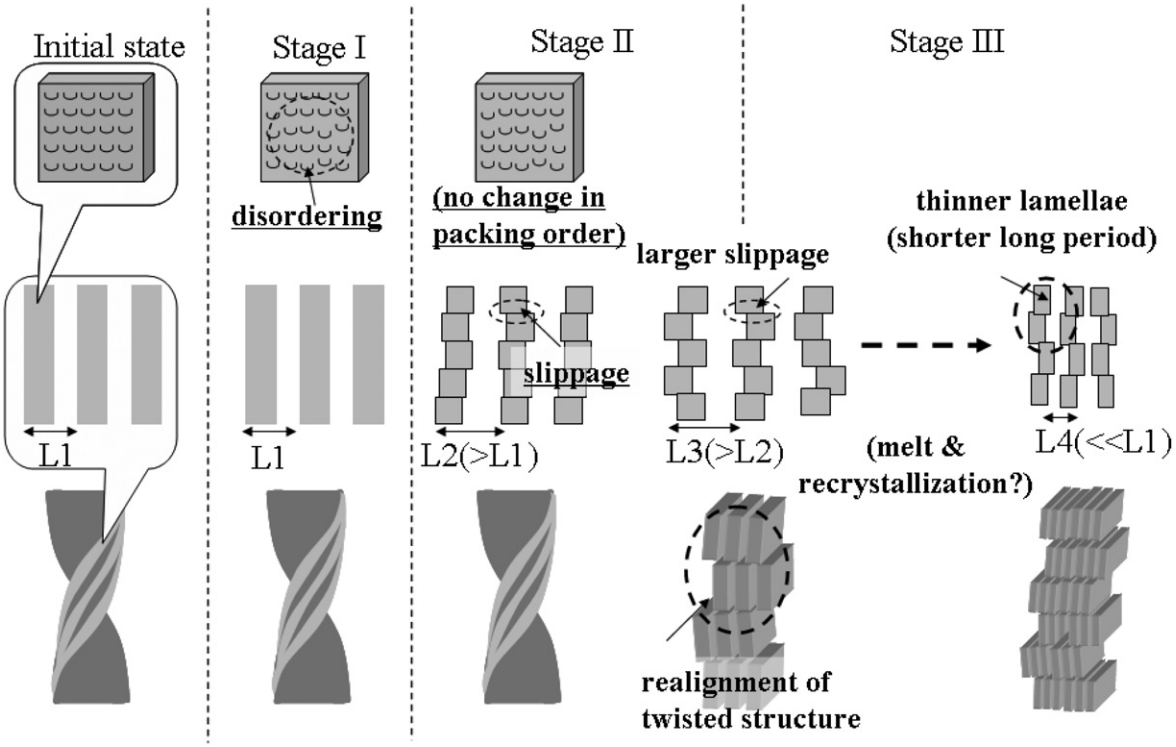

Fig. 12. Structural deformation model during drawing of PCL/PVB.

in-situ SAXS–WAXS–POM measurements during drawing at an inclined lamella region of a spherulite.

Next, the lamella reconstruction mechanism which occurs in stage III is discussed. In PCL/PVB, it is difficult to explain the drastic change in the long period structure and its thermal property without considering the melting and recrystallization mechanism. Furthermore, as shown in Fig. 8, the drastic reconstruction of the long period structure occurs in a very short time, and the moment of melting and recrystallization may be difficult to determine by an ex-situ method and spatially averaged experimental techniques. Our microbeam experimental results strongly indicate that the mechanical melting and recrystallization process occurs in stage III, where the correlation function at the end of stage III showed much stronger correlation than that at the beginning of stage III.

However, it should be also noted that the melting and recrystallization mechanism may not be a universal mechanism in other polymer systems. In PE, it is considered that melting and recrystallization will only occur at higher temperature than 95 °C [9]. Furthermore, the deformation manner itself strongly depends on the type of polymer and the drawing conditions. For example, in our previous study, the deformation behavior of an iPP spherulite was investigated by microbeam SAXS–WAXS–POM simultaneous measurement [30]. In this case, the long period after drawing at 154 °C was thinner than that of the initial state, which was formed by isothermal crystallization at 128 °C, and a similar phenomenon in iPP was also reported by other authors [57]. In the case of iPP, we concluded that no evidence of melting and recrystallization was observed and that a simple fragmentation process may be the main mechanism in iPP deformation under our experimental conditions. Interestingly, in iPP, the decrease in the long period occurs with the 'ordering' of lamella stacking, while the decrease in the long period in PCL/PVB occurs with the 'disordering' of lamella stacking. This difference also strongly indicates that the mechanism of reconstruction of lamella long period is completely dependent on the type of polymer and the drawing conditions. In order to fully understand the essential point of the deformation mechanism of lamella rearrangement, we must systematically perform microbeam SAXS–WAXS experiments for various polymer spherulites and classify the deformation mechanism, which may be strongly dependent on the crystal structure (for example, the possibility of sliding diffusion) and drawing conditions (for example, the relationship between the characteristic relaxation time of the polymer chain and the drawing rate).

5. Conclusion

We have performed in-situ microbeam SAXS–WAXS–POM simultaneous measurements during the drawing of PCL/PVB banded spherulites. From the experimental results, we propose a deformation model for PCL/PVB banded spherulites with four stages. In stage I, disordering of the crystalline structure occurs. In stage II, the disordering of the crystalline structure ceases and disordering of the stacking and coarse slippage of the lamellae occur. In stage III, after the breakdown of the twisting lamella structure, the reconstruction of a long period structure occurs. In stage IV, further lamella slippage occurs. In addition, our results show no evidence of fine slippage during the drastic decrease in the long period, which is sometimes considered as a key structural change in the proposed mechanisms other than the melting and recrystallization mechanism. Thus, our results strongly indicate that the melting and recrystallization mechanism is dominant during the lamella reconstruction of PCL/PVB. We have demonstrated that microbeam SAXS–WAXS–POM simultaneous measurement clearly shows the pathway of structure deformation in a complex hierarchical structure.

Acknowledgement

The authors thank Drs. K. Inoue and N. Ohta (JASRI) for their support in the setup of the microbeam experiment. This experiment

was performed under the approval of SPring-8 Program Advisory Committee (Proposal Numbers: 2005A0705, 2005B0155) and the approval of the Photon Factory Program Advisory Committee (Proposal No. 2004G268).

References

[1] Hiss R, Hobeika S, Lynn C, Strobl G. Macromolecules 1999;32:4390.
[2] Hong K, Rastogi A, Strobl G. Macromolecules 2004;37:10165.
[3] Corneliussen R, Peterlin A. Die Makromol Chemie 1967;105:193.
[4] Peterlin A. J Mater Sci 1971;6:490.
[5] Kanig G. J Cryst Growth 1980;48:303.
[6] Adams WW, Yang D, Thomas EL. J Mater Sci 1986;21:2239.
[7] Wignall GD, Wu W. Polym Commun 1983;54:354.
[8] Flory PJ, Yoon DY. London. Nature 1978;272:226.
[9] Sadler DM, Barham PJ. Polymer 1990;31:36.
[10] Wu W, Wignall GD, Mandelkern L. Polymer 1992;33:4137.
[11] Butler MF, Donald AM, Ryan AJ. Polymer 1998;39:781.
[12] Galeski A, Bartzak Z, Argon AS, Cohen RE. Macromolecules 1992;25:5705.
[13] Young RJ, Bowden PB, Ritchie JM, Rider JG. J Mater Sci 1973;8:23.
[14] Keller A, Pope DP. J Mater Sci 1971;6:453.
[15] Chuah HH, Lin JS, Porter RS. Macromolecules 1986;19:2732.
[16] Hu WG, Rohr KS. Acta Polym 1999;50:271.
[17] Hobeika S, Men Y, Strobl G. Macromolecules 2000;33:1827.
[18] Koike Y, Cakmak M. Macromolecules 2004;37:2171.
[19] Song Y, Nitta K, Nemoto N. Macromolecules 2003;36:8066.
[20] Liu TM, Juska TD, Harrison IR. Polymer 1986;27:247.
[21] Unwin AP, Bower DI, Ward IM. Polymer 1985;26:1605.
[22] Ballard DGH, Cheshire P, Janke E, Nevin A, Schelten J. Polymer 1982;23:1875.
[23] Sakurai T, Nozue Y, Kasahara T, Mizunuma K, Yamaguchi N, Tashiro K, et al. Polymer 2005;46:8846.
[24] Jiang Z, Tang Y, Men Y, Enderle HF, Lilge D, Roth SV, et al. Macromolecules 2007;40:7263.
[25] Kakudo M, Kasai N. X-ray diffraction by polymers (original title in Japanese). Tokyo: Maruzen; 1968. p. 298.
[26] Keith HD, Padden FJ. J Appl Phys 1966;37:4013.
[27] Keller A. J Polym Sci 1955;17:291.
[28] Saracovan I, Keith HD, Manley RJ, Brown GR. Macromolecules 1999;32:8918.
[29] Keith HD, Padden FJ, Russell TP. Macromolecules 1989;22:666.
[30] Nozue Y, Shinohara Y, Ogawa Y, Sakurai T, Hori H, Kasahara T, et al. Macromolecules 2007;40:2036.
[31] Riekel C, Muller M, Vollrath F. Macromolecules 1999;32:4464.
[32] Davies RJ, Burghammer M, Riekel C. Macromolecules 2005;38:3364.
[33] Davies RJ, Burghammer M, Riekel C. Macromolecules 2007;40:5038.
[34] Gazzano M, Focarete ML, Riekel C, Scandola M. Biomacromolecules 2000;1:604.
[35] Nozue Y, Kurita R, Hirano S, Kawasaki N, Ueno S, Iida A, et al. Polymer 2003;44:6397.
[36] Nozue Y, Hirano S, Kawasaki N, Ueno S, Yagi N, Nishi T, et al. Polymer 2004;45:8593.
[37] Torre J, Cortazar M, Gomez MA, Marco C, Ellis G, Riekel C, et al. Macromolecules 2006;39:5564.
[38] Shimamura K, Murakami S, Tsuji M, Katayama K. Nihon Rheology Gakkai-shi 1979;7:42.
[39] Point JJ. Bull Acad R Belg 1955;41:982.
[40] Hobbs JK, Binger DR, Keller A, Barham PJ. J Polym Sci B Polym Phys 2000;38:1575.
[41] Ho RM, Ke KZ, Chen M. Macromolecules 2000;33:7529.
[42] Saracovan I, Cox JK, Revol JF, Manley RJ, Brown GR. Macromolecules 1999;32:717.
[43] Sasaki S, Sakaki Y, Takahara A, Kajiyama T. Polymer 2002;43:3441.
[44] Janimak JJ, Markey L, Stevens GC. Polymer 2001;42:4675.
[45] Wang Z, An L, Jiang W, Jiang B, Wang X. J Polym Sci B Polym Phys 1999;37:2682.
[46] Patel D, Bassett DC. Polymer 2002;43:3795.
[47] Fujiwara Y. J Appl Polym Sci 1960;4:10.
[48] Bassett DC, Hodge AM. Proc R Soc London 1981;A377:25.
[49] Bassett DC. Philos Trans R Soc London 1994;A348:29.
[50] Keith HD, Padden FJ. Polymer 1984;25:28.
[51] Keith HD, Padden FJ. Macromolecules 1996;29:7776.
[52] Singfield KL, Klass JM, Brown GR. Macromolecules 1995;28:8006.
[53] Singfield KL, Hobbs JK, Keller A. J Cryst Growth 1998;183:683.
[54] Inoue K, Oka T, Suzuki T, Yagi N, Takeshita K, Goto S, et al. Nucl Instrum Methods 2001;A467–468:674.
[55] Amemiya Y, Ito K, Yagi N, Asano Y, Wakabayashi K, Ueki T. Rev Sci Instrum 1995;66:2290.
[56] Schrauwen BAG, Janssen RPM, Govaert LE, Meijer HEH. Macromolecules 2004;37:6069.
[57] Zuo F, Keum JK, Chen X, Hsiao BS, Chen H, Lai SY, et al. Polymer 2007;48:6867.